Eur. Phys. J. D **50**, 185–191 (2008)
DOI: 10.1140/epjd/e2008-00213-1

THE EUROPEAN PHYSICAL JOURNAL D

Filamentation of chirped pulses on long-range atmospheric paths

V.Y. Fedorov[a], S.A. Shlenov, and V.P. Kandidov

International Laser Center and Physics Department, Lomonosov Moscow State University, Leninskie gory, 119991 Moscow, Russia

Received 23 June 2008 / Received in final form 29 September 2008 / Published online 14 November 2008

Abstract. A semi-analytical method has been proposed to analyse filamentation of powerful femtosecond laser pulses. The method is based on the multiplicative representation of pulse in space and time domains in the pre-filamentation region, where Kerr self-focusing is dominated. Systematic error due to disregarding phase self-modulation in this region has been analysed and a criterion has been suggested to determine the furthest limit of this region. It is shown that if the limit of the pre-filamentation region is set according to this criterion, the errors in calculations of filament and plasma channels parameters do not exceed 10%. The method substantially reduces computer resources needed to make simulations, in the case of highly chirped pulses propagating in randomly inhomogeneous media, in particular, along lengthy paths in turbulent atmosphere.

PACS. 42.65.Jx Beam trapping, self-focusing and defocusing; self-phase modulation – 42.68.Ay Propagation, transmission, attenuation, and radiative transfer

1 Introduction

High intensity laser radiation in a femtosecond pulse filament and supercontinuum generation make it possible to use filamentation phenomenon for remote sensing of atmosphere [1] and surface analysis [2]. The delivery of high powers at remote locations is one of the most critical problems for these applications. Pulses that are tens or hundreds of femtoseconds in duration have a wide spectral range and at long-range atmospheric paths undergo noticeable dispersion spreading. To counteract this effect the precompensation of group velocity dispersion is used [3]. Since air has normal group velocity dispersion at wavelength of Ti:sapphire laser, a negative chirp will result in pulse compression at some distance due to recombination of its Fourier components. Filamentation of chirped pulses generally starts at greater distances. Filament formation in ultrashort chirped pulses propagating vertically in the atmosphere was observed at altitudes of several kilometers [1,4]. On horizontal atmospheric paths, filament plasma channels were detected at distances of several hundred meters and hot-spots in pulse cross-section were observed at distances more than 2 km from the laser system output [5].

Numerical simulations are useful tools for understanding femtosecond laser pulse filamentation. However, computer simulation of a chirped pulse propagation on a kilometer-range atmospheric path often requires unreasonable computing time. Furthermore, the range of typical scales of laser field variations under filamentation expands on several orders and it is necessary to use extremely high computer capacities. A reduced 2D model was suggested [6] to decrease computer requirements. This model reduces the number of computational grid nodes in time domain by freezing suitable temporal dependencies of the wave field. It has been used to study multifilamentation in the air [7].

A ray-tracing technique to simulate the nonlinear propagation of ultra-short pulses has been proposed [8]. The initial beam cross section is sampled transversally into small cells. Typically 100 rays are launched from each cell bearing a power determined by its position in the beam profile. In each case, the total power of all rays contained in each cell is used to compute the local nonlinear change of refractive index. The trajectory of each ray is calculated analytically using classical Fresnel formula. In this approach, diffraction is not taken into account, and the pulse is averaged temporally. Multiphoton ionisation is neglected, as well as group velocity dispersion.

Two regimes of ultrashort, high-power pulse propagation are considered [9]. At the prefilamentation region, where pulse peak intensity is low in comparison with the photoionisation threshold, it is supposed that the pulse keeps its Gaussian shape in time and space domain. As a result a set of self-consistent coupled equations for the pulse amplitude, phase, curvature, and spot size were derived. When intensity reaches the photoionisation threshold, the full system of equations, which describes pulse evolution and plasma generation, is solved.

[a] e-mail: fedoroff_v@mail.ru

The requirement of gauss shape in pulse cross-section imposes some restrictions, for example, it makes it hard to consider the multifilamentation of pulses with initial perturbations and pulse propagation in the turbulent atmosphere. Earlier [10] we suggested a method, which was used for numerical investigation of chirped pulse propagation on kilometer-range paths in the turbulent atmosphere.

In the present paper we develop a semi-analytical method for computer simulation of femtosecond pulse filamentation. This method is based on splitting time and spatial dependencies of light field at the prefilamentation region. Evolution of pulse time parameters is described analytically in linear approximation at this region. Evolution of the pulse in space domain is calculated numerically taking into account Kerr self-focusing and allowing pulse shape transformations in its cross-section due to both nonlinearity and random fluctuations of the refractive index of the medium.

2 Pulse filamentation model

Femtosecond pulse propagation is described by the following equation for the slowly varying amplitude of the electric field $E(x,y,t,z)$ [11,12]

$$2ik_0\frac{\partial E}{\partial z} = \Delta_\perp E - k_0 k_\omega^{''}\frac{\partial^2 E}{\partial t^2} + \frac{2k_0^2}{n_0}\Delta n_k(x,y,t,z)E + \frac{2k_0^2}{n_0}\Delta n_p(x,y,t,z)E + \frac{2k_0^2}{n_0}\tilde{n}(x,y,z)E - ik\alpha E \quad (1)$$

where k_0 is the wave number, $k_\omega^{''} = \partial^2 k/\partial\omega^2$, ω is the central frequency of the pulse spectrum, n_0 is the undisturbed linear refractive index of air. The first two terms on the right-hand side (1) describe the pulse diffraction and second order dispersion. The Kerr nonlinearity of air is represented by the third term. The contribution of plasma nonlinearity is described by the fourth term. The turbulent fluctuations of the air refractive index $\tilde{n}$ are responsible for the random character of filamentation. The last term on the right-hand side (1) account for pulse energy losses due to photoionisation. This equation does not include the high-order material dispersion terms and the time derivative of nonlinearity which accounts for the effect of the pulse front self-steepening.

The Kerr contribution Δn_k to the refractive index can be written as

$$\Delta n_k(x,y,t,z) = n_2 I(x,y,t,z) \quad (2)$$

where $I = \frac{\varepsilon_0 c n_0}{2}|E|^2$ is the pulse intensity, ε_0 is the electric constant. The cubic nonlinearity coefficient of the air refractive index is equal to $n_2 = 4\times10^{-23}$ m^2/W [13]. The non-stationary contribution to Kerr nonlinearity from the stimulated Raman scattering on rotational transitions of air molecules can be taken into account by introducing the effective nonlinearity coefficient n_2 for a short pulse [14].

Refractive index changes in plasma, produced upon photoionisation of air molecules in the intense laser field, can be expressed as

$$\Delta n_p(x,y,t,z) = -\frac{\omega_p^2}{2n_0\omega^2} \quad (3)$$

where $\omega_p^2(x,y,t,z) = e^2 N_e(x,y,t,z)/\varepsilon_0 m$ is the square of the plasma frequency, e and m are the electron charge and mass respectively and N_e is the density of free electrons. This is described by the rate equation

$$\frac{\partial N_e}{\partial t} = R(I)(N_0 - N_e) \quad (4)$$

where N_0 is the concentration of neutral molecules and $R(I)$ is the ionisation rate, which is determined using the Perelomov-Popov-Terent'ev model [15].

Fluctuations of the refractive index in the atmosphere $\tilde{n}(x,y,z)$ produce perturbations of the light field phase in a pulse cross-section leading to the random character of filamentation. Contribution of $\tilde{n}$ to laser field phase is described within the framework of the model of phase screens [12].

For a laser pulse with Gaussian intensity distribution in space, time and quadratic phase modulation, complex amplitude of the light field $E(x,y,t,z=0)$ at the exit of the laser system has the following form:

$$E = E_0\sqrt{\frac{\tau_0}{\tau_{\delta 0}}}\exp\left(-\frac{x^2+y^2}{2a_0^2} - \frac{t^2}{2\tau_{\delta 0}^2} + i\frac{\delta t^2}{2}\right) \quad (5)$$

where a_0 is the radius of the pulse cross-section, $\tau_{\delta 0}$ is duration of the chirped pulse, and, τ_0 and E_0 are duration and amplitude of the corresponding transform-limited pulse. Parameter of the phase modulation δ can be written as

$$\delta = -\frac{\sqrt{(\tau_{\delta 0}/\tau_0)^2 - 1}}{\tau_{\delta 0}^2}. \quad (6)$$

Negatively chirped pulse ($\delta < 0$) propagating in a medium with normal dispersion will compress to transform-limited one at length L_{com} equal to

$$L_{com} = -\frac{\tau_0^2\tau_{\delta 0}^2\delta}{|k_\omega^{''}|}. \quad (7)$$

The dispersion length $L_{disp} = \tau_0^2\Big/\left|k_\omega^{''}\right|$ of the transform-limited pulse is also a characteristic of the problem. Pulse duration $\tau_{\delta 0}$ and parameter δ can be expressed in terms of introduced parameters L_{com} and L_{disp}

$$\tau_{\delta 0} = \tau_0\sqrt{1+\left(\frac{L_{com}}{L_{disp}}\right)^2}; \quad \delta = -\frac{L_{com}}{\tau_{\delta 0}^2 L_{disp}}. \quad (8)$$

3 Semi-analytical method

The suggested semi-analytical method is based on the fact that a considerable part of the propagating path, pulse intensity $I(z)$ is much lower than the ionisation threshold I_{ion} in the air ($I_{ion} \sim 10^{13}$ W/cm^2):

$$I\left(z \leqslant z_{prefil}\right) \ll I_{ion}, \tag{9}$$

where z_{prefil} is a prefilamentation region boundary. In the initial stage of pulse propagation, referred to as a prefilamentation region, there is no plasma generation ($\Delta n_p = 0$). The extension of the prefilamentation region is especially large for pulses with initial phase modulation, whose peak power is lower or close to the self-focusing critical power.

This assumes that pulse time profile variations over the whole region of the prefilamentation result solely from group velocity dispersion in the air, with phase self-modulation being negligible. The slowly varying amplitude of the light field $E(x, y, t, z)$ has been represented in the form

$$E(x, y, t, z) = E_{sp}(x, y, z)T(t, z) \tag{10}$$

where $T(t, z)$ is solution of the linear second-order dispersion equation

$$2ik_0\frac{\partial T(t,z)}{\partial z} = -k_0 k_\omega^{''}\frac{\partial^2 T(t,z)}{\partial t^2}. \tag{11}$$

The analytical solution of equation (11) for Gaussian pulse with initial phase modulation is

$$T(t,z) = \sqrt{\frac{\tau_0}{\tau_\delta(z)}}\exp\left(-\frac{t^2}{2\tau_\delta^2(z)} + i\varphi(t,z)\right). \tag{12}$$

The variations of pulse duration $\tau_\delta(z)$ and phase $\varphi(t, z)$ with propagation distance are given by [16]

$$\tau_\delta(z) = V(z)\tau_{\delta 0}, \tag{13}$$

$$\varphi(t,z) = \frac{1}{2V(z)}\left[k_\omega^{''}z\left(\delta^2 + \tau_{\delta 0}^{-4}\right) + \delta\right]t^2 - \frac{1}{2}\mathrm{arctg}\left(\frac{k_\omega^{''}z}{\tau_{\delta 0}^2\left(1 + \delta k_\omega^{''}z\right)}\right), \tag{14}$$

$$V(z) = \left(1 + \delta k_\omega^{''}z\right)^2 + \left(\frac{k_\omega^{''}z}{\tau_{\delta 0}^2}\right)^2. \tag{15}$$

Function $E_{sp}(x, y, z)$ describes field changes over pulse cross-section in accordance with (5), (10), (12) and $E_{sp}(x = 0, y = 0, z = 0) = E_0$. Substituting $E(x, y, t, z)$ in the form (10) into (1) and neglecting phase self-modulation, results in the following propagation equation for $E_{sp}(x, y, z)$ over prefilamentation region ($\Delta n_p = 0$)

$$2ik_0\frac{\partial E_{sp}(x,y,z)}{\partial z} = \Delta_\perp E_{sp}(x,y,z) + \frac{2k_0^2}{n_0}\frac{1}{2}n_2 \times I(x,y,t=0,z)E_{sp}(x,y,z) + \frac{2k_0^2}{n_0}\tilde{n}(x,y,z)E_{sp}(x,y,z), \tag{16}$$

where $I(x, y, t = 0, z)$ is intensity in the pulse central time layer, which is given by

$$I(x,y,t=0,z) = \frac{\varepsilon_0 c n_0}{2}\left|E_{sp}(x,y,z)T(t=0,z)\right|^2. \tag{17}$$

Equations (11) and (16) describe evolution of the complex laser field amplitude over the prefilamentation region. According to the model the laser pulse keeps its Gaussian form (12) in time domain. In addition, distribution of the light field over pulse cross-section $E_{sp}(x, y, z)$ is constant for all time layers. Propagation (16) is solved numerically. As a result the complex amplitude $E(x, y, z_{prefil})$ is determined at the boundary of the prefilamentation region.

Beyond the prefilamentation region ($z > z_{prefil}$), laser field $E(x, y, t, z)$ is described by (1) and the initial value $E(x, y, t, z_{prefil})$ obtained at the boundary of the prefilamentation region. In accordance with (10), (12) $E(x, y, t, z_{prefil})$ can be written as

$$E(x,y,t,z_{prefil}) = E_{sp}(x,y,z_{prefil})\sqrt{\frac{\tau_0}{\tau_\delta(z_{prefil})}} \times \exp\left(-\frac{t^2}{2\tau_\delta^2(z_{prefil})} + i\varphi(z_{prefil})\right). \tag{18}$$

Thus, this semi-analytical method allows consideration of simulations in single pulse time layer at the initial stage of the pulse propagation (over the prefilamentation region). Variations of pulse time profiles are described analytically within the limits of linear dispersion theory.

Note that suggested semi-analytical method can be used to describe effects, which lead to changes of the laser field over pulse cross-section at the prefilamentation stage. Particularly, variations of the air refractive index due to atmosphere turbulence and aerosol scattering can be considered. In addition, initial field distribution (5) can reproduce initial perturbations over pulse cross-section at the exit of the laser system. Beyond the prefilamentation region at $z > z_{prefil}$ other effects such as high order dispersion, pulse front self-steepening and the delayed component in the Kerr response, can be included in propagation (1).

Application of the semi-analytical method significantly reduces the required CPU time and memory in numerical computation, while simulating the chirped pulses filamentation at long-range atmospheric paths under turbulent conditions. The introduction of spatial perturbations over pulse cross-section yields smaller integration step Δz along the evolutional coordinate z. The split-step procedure, commonly used for the numerical solution of (1), requires the step Δz be less than the diffraction length of the smallest spatial scale of light field variation [17]. Initial perturbations of the laser beam and atmospheric inhomogenity of the optical parameters imply that the pulse propagation, including prefilamentation region, should be simulated using small integration step Δz. Simulation of the pulse propagation with small step Δz and high temporal resolution over long distance requires too many computational resources. The semi-analytical method reduces

computational costs because it propagates only one, central time layer of the pulse over the prefilamentation region. Integration of all time layers of the pulse is only used over relatively short distance in the vicinity of the filament start, where the plasma nonlinearity and pulse splitting play significant role.

4 Simulation of pulse propagation

The computational efficiency of the semi-analytical method depends on the prefilamentation region boundary value z_{prefil}, which is a free parameter in this method. In order to reveal the effect of z_{prefil} value on calculated filament parameters, we performed numerical simulations of Gaussian pulse propagation in the absence of atmospheric turbulence ($\tilde{n} = 0$) and initial light field perturbations. Transform-limited pulse duration at 800 nm wavelength was $\tau_0 = 100$ fs, pulse energy $W = 5.6$ mJ and beam radius $a_0 = 1$ cm. Thus, the initial peak power P_0 of the transform-limited pulse is 13 times above the critical power P_{cr} for self-focusing in the air. The initial duration of the stretched pulse with phase modulation was $\tau_{\delta 0} = 340$ fs, and as a consequence, the peak power $P_{\delta 0}$ of the chirped pulse amounted to $3.8P_{cr}$. The compression length of the chirped pulse was equal to $L_{com} = 2000$ m. The simulations of axially symmetric beam propagation were carried out.

The dependencies of the pulse peak intensity $I_{peak}(r, t, z)$ on propagation distance z up to the point where I_{peak} reaches the plasma generation threshold are shown (Fig. 1). These dependencies were obtained by using the semi-analytical method with different values of z_{prefil} parameter and numerical solution of (1) over the whole propagation path. The semi-analytical method (16) was numerically integrated up to $z = z_{prefil}$ (where $z_{prefil} = 115$ or 200 m) and then for distances $z > z_{prefil}$, full propagation equation (1) was numerically integrated. When pulse propagation commences, a slow intensity increase occurs due to pulse compression and weak self-focusing of the pulse with peak power only slightly higher than the critical power ($P_{\delta 0}/P_{cr} \sim 3.8$). It is then replaced by an avalanche growth while approaching the plane of nonlinear focus. The distance to that plane can be considered a filament start distance z_{fil} in a regular medium. It can be seen that the semi-analytical method gives an underestimated value of z_{fil} distance in comparison with the result of the numerical solution of full propagation (1). Applying the semi-analytical method leads to an earlier filament appearance. The error margin in determining the filament start distance z_{fil} by the semi-analytical method does not exceed 2%. Analysis carried out with different values of pulse parameters, showed that the systematic error of the semi-analytical method does not exceed 10%. The error in the determination of z_{fil} is weakly dependent on z_{prefil} parameter. A twofold decrease in z_{prefil} value (from 200 m to 115 m) has little effect on accuracy of the filament start distance (Fig. 1).

To estimate influence of z_{prefil} parameter on the calculated filament radius, the peak value of fluency inside

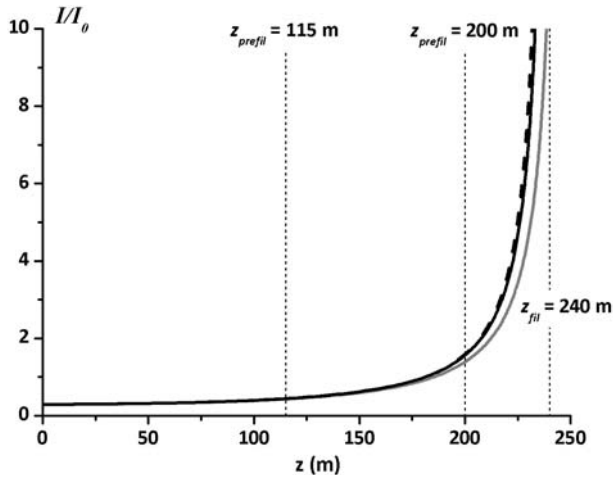

Fig. 1. Evolution of pulse peak intensity $I(z)$. Gray curve; numerical solution of (1). Black curve; semi-analytical method with $z_{prefil} = 115$ m (solid) and 200 m (dashed).

a filament and concentration of the electrons in plasma channel one can compare the results in Figure 2 obtained by the semi-analytical method and fully numerical solution. Two values of $z_{prefil} = 115$ and 200 m were used as boundaries of the prefilamentation region. The curves corresponding to the semi-analytical method were shifted along z coordinate to align the filament start position for the convenience of comparison analysis. The changes of filament parameters with distance, obtained by both methods are close to each other. In the semi-analytical method the peak values of filament parameters are slightly higher (Fig. 2). This difference increases if the prefilamentation region boundary z_{prefil} is chosen closer to the filament start z_{fil}. It is also noted there are slower variations in filament parameters along the propagation axis when z_{prefil} increases.

Spatio-temporal distributions of intensity $I(r, t)$ obtained by the semi-analytical method and fully numerical solution are shown in Figure 3. Essential distortions of the pulse Gaussian profile take place only in the vicinity of a filament start z_{fil}. The most substantial difference between intensity distributions obtained by each method is the time domain. The pulse duration obtained by fully numerical simulations is noticeably smaller than the semi-analytical method at distances $z > 150$ m. This is explainable as phase self-modulation is omitted over the prefilamentation region in the semi-analytical method.

5 Accuracy analysis

For a quantitative analysis of the pulse profile deviations from Gaussian shape function $F(t, z)$ can be used, which is defined by

$$F(t,z) = \sqrt{\left|\ln\left(\frac{I(t,z)}{I(0,z)}\right)\right|_{r=0}}. \qquad (19)$$

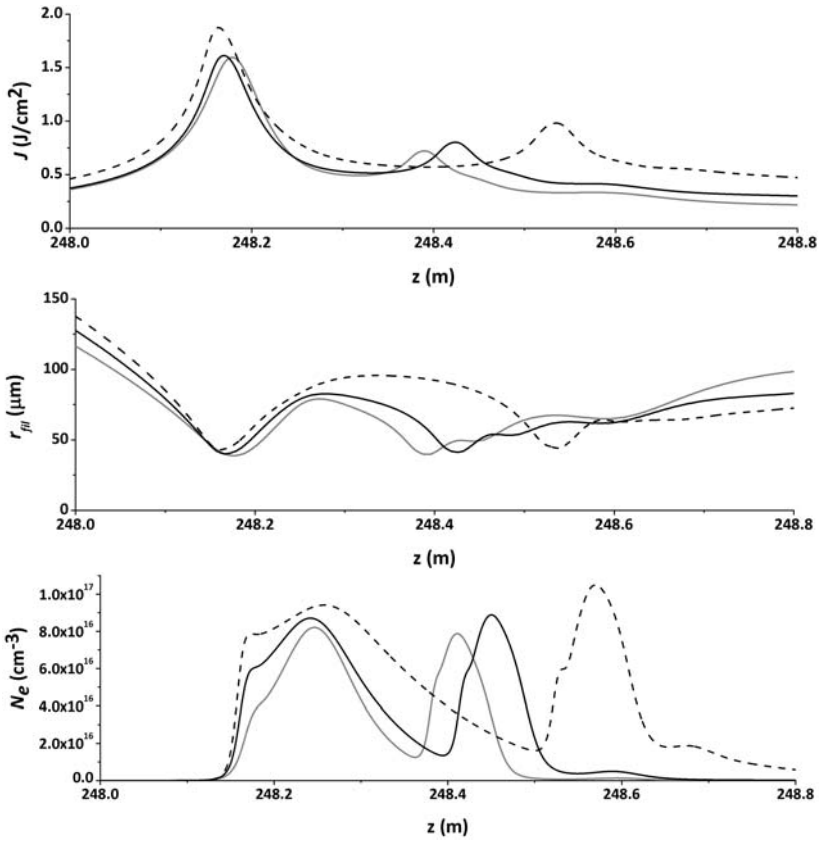

Fig. 2. Filament parameters in the vicinity of its start: peak fluence (a), radius (b), electron concentration in plasma channel (c). Gray curve; numerical solution of (1). Black curve; semi-analytical method with $z_{prefil} = 115$ m (solid) and 200 m (dashed).

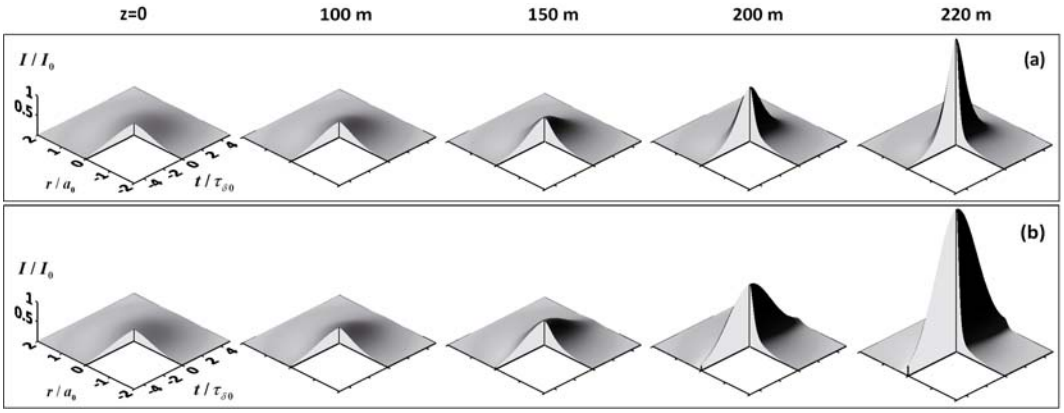

Fig. 3. Spatio-temporal intensity distribution in a laser pulse at several distances z; (a) fully numerical solution, (b) semi-analytical method with $z_{prefil} = 200$ m.

It is easy to see that for a Gaussian shape pulse (12) function $F(t, z)$ is linearly dependent on t at an arbitrary distance z^*

$$F(t, z^*) = \frac{t}{\tau_\delta(z^*)}. \tag{20}$$

Tangent of the slope angle $\theta(z^*)$ to t axis of this linear function is equal to inverse pulse duration $\tau_\delta^{-1}(z^*)$ at the distance z^*. Deviation from a Gaussian pulse shape on the beam axis ($z^* = 0$) can be characterised by the deviation of $F\left(t/\tau_\delta(z^*), z^*\right)$ from linear dependence with $\theta(z^*) = \pi/4$. Function $F\left(t/\tau_\delta(z^*), z^*\right)$, calculated by a fully numerical solution, is plotted in Figure 4 for several distances z^*. The initially Gaussian profile ($z^* = 0$) of the pulse is changed with distance due to phase self-modulation, which is clearly seen from deflecting $F\left(t/\tau_\delta(z), z\right)$ graph from a straight line. The rise of slope angle $\theta(t, z)$ of the graph in the vicinity of point $t = 0$ is evidence of significant shortening of characteristic time scale in the central part of the pulse. This is in comparison with dependence

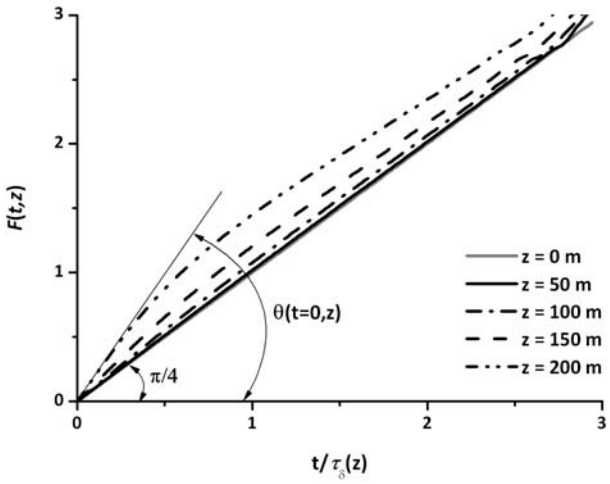

Fig. 4. $F(t,z)$ function (19), which shows pulse shape deviation from the Gaussian shape at several distances along the propagation axis.

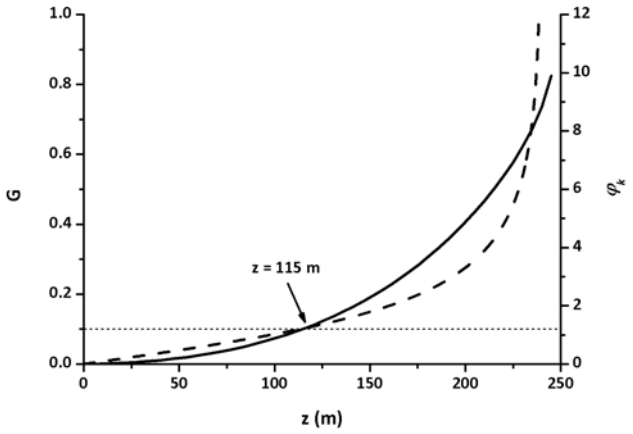

Fig. 5. Calculated parameter G (solid curve) and the Kerr nonlinear phase shift φ_k (dashed curve) versus propagation distance z. The prefilamentation region boundary is marked by an arrow.

determined by the linear dispersion. Figure 3 illustrates a noticeable temporal profile sharpening in the central part of the pulse at the distances $z = 200$ and 220 m, which is clearly distinguished from a Gaussian profile (12).

Deviation from a Gaussian pulse shape can be quantified with the parameter $G(z)$

$$G(z) = \left| \frac{\theta(t=0,z) - \pi/4}{\pi/4} \right|. \tag{21}$$

Suppose that the pulse time shape remains Gaussian if $G(z)$ is less or equal to 0.1. The relative deviation of the slope angle $\theta(t=0,z)$ of the function $F\left(t/\tau_\delta(z), z\right)$ from $\pi/4$ does not exceed 0.1

$$G(z) \leqslant 0.1. \tag{22}$$

Note that condition (22) is rather strong because the maximum deviation of the pulse from a Gaussian shape (or parameter G from zero) is estimated in the central part of the pulse at $t = 0$. In the pulse wings, where nonlinearity is smaller and linear dispersion plays main role in variation the pulse shape parameter G, is close to zero.

Dependence of parameter $G(z)$ on propagation distance z is shown in Figure 5. The value of this parameter does not exceed 0.1 and in accordance with criterion (22) the pulse holds its Gaussian shape over distances up to 115 m. This distance can be taken as a boundary of the prefilamentation region z_{prefil} in the semi-analytical method. At $z = 115$ m the pulse peak intensity I_{peak} is 1.5 times higher than initial intensity of the chirped pulse and 2.5 times lower than the intensity of the corresponding transform-limited pulse I_0. At this distance I_{peak} is equal to 4.4×10^9 W/cm^2, which is still significantly lower than the photoionisation threshold I_{ion} in the air. Note that at the distance where pulse peak intensity is close to the photoionisation threshold I_{ion}, the value of parameter G is greater than 0.85.

The calculation of parameter G is based on fully numerical solution of (1) and therefore it is a posteriori estimation. It is of practical interest to make a priori estimation of parameter G while solving equations (11) and (16) in the semi-analytical method. Since the pulse profile deviation from Gaussian shape is due to nonlinearity, the value of nonlinear phase shift or B-integral can be chosen as a priori estimation

$$\varphi_k(z) = \int \frac{k_0 n_2}{n_0} I_0(z) dz. \tag{23}$$

On-axis intensity of the pulse central layer $I_0(z) = I(x=0, y=0, t=0, z)$ can be calculated by formula (17). Variation of the nonlinear phase shift $\varphi_k(z)$ with distance z, obtained in the semi-analytical method, is shown in Figure 5. At the distance $z = 115$ m phase shift $\varphi_k(z_{prefil})$ is equal to 1.2. The B-integral value can be used to determine the boundary of the prefilamentation region z_{prefil} in the semi-analytical method. The current value of $\varphi_k(z)$ can be easily monitored in numerical simulations of pulse propagation over the prefilamentation region.

The semi-analytical method allows decreases calculation time by approximately 40% compared to fully numerical solution. The effectiveness of the method depends on the length of prefilamentation region. This distance in turn depends on the value of initial phase modulation (chirp) of the pulse. Where there is a strong phase modulation, the initial peak power of the chirped pulse can be lower than the critical power for self-focusing. The intensity growth along the propagation path is possible only due to chirped pulse compression in the air. In this case the first stage of the pulse propagation is not exposed to phase modulation caused by the Kerr effect. It allows extension of the prefilamentation region. In our simulations of chirped pulse filamentation at kilometer-range paths under realistic conditions we reduced calculation time be up to 90%. The use of the semi-analytical method allowed simulation of the filamentation of femtosecond laser pulse over a 1.5 km path in turbulent atmosphere [10].

6 Conclusions

A semi-analytical method for the problem of filamentation of high power femtosecond laser pulse with initial phase modulation at long-range paths was developed. The method is based on multiplicative representation of the light field in the prefilamentation region. In this region spatial variation of the field is determined by the Kerr nonlinearity and refractive index fluctuations, while temporal evolution is determined by the pulse compression in linear dispersive medium. The method systematic error was investigated and a criterion to choose the boundary of the prefilamentation region was proposed. It was shown that determination of the prefilamentation region in accordance with the proposed criterion leads to errors in basic parameters of the filament and plasma channel which do not exceed 10%. The consumption of computer resources was drastically reduced. The use of the semi-analytical method to model filamentation of femtosecond pulses in the atmosphere is most effective for highly chirped pulses and transform-limited pulses with peak power a little higher than the critical power for self-focusing.

References

1. J. Kasparian, M. Rodriguez, G. Mejean, J. Yu, E. Salmon, H. Wille, R. Bourayou, S. Frey, Y.-B. Andre, A. Mysyrowicz, R. Sauerbrey, J.-P. Wolf, L. Woste, Science **301**, 61 (2003)
2. P. Rohwetter, K. Stelmaszczyk, L. Woste, R. Ackermann, G. Mejean, E. Salmon, J. Kasparian, J. Yu, J.-P. Wolf, Spectrochim. Acta B **60**, 1025 (2005)
3. H. Wille, M. Rodriguez, J. Kasparian, D. Mondelain, J. Yu, A. Mysyrowicz, R. Sauerbrey, J.-P. Wolf, L. Woste, Eur. Phys. J. Appl. Phys. **20**, 183 (2002)
4. M. Rodriquez, R. Bourayou, G. Mejean, J. Kasparian, J. Yu, E. Salmon, A. Scholz, B. Stecklum, J. Eisloffel, U. Laux, A.P. Hatzes, R. Sauerbrey, L. Woeste, J.-P. Wolf, Phys. Rev. E **69**, 036607 (2004)
5. G. Mechain, C. D'Amico, Y.-B. Andre, S. Tzortzakis, M. Franco, B. Prade, A. Mysyrowicz, A. Couairon, E. Salmon, R. Sauerbrey, Opt. Commun. **247**, 171 (2005)
6. S. Skupin, L. Berge, U. Peschel, F. Lederer, G. Mejean, J. Yu, J. Kasparian, E. Salmon, J.P. Wolf, M. Rodriguez, L. Woste, R. Bourayou, R. Sauerbrey, Phys. Rev. E **70**, 046602 (2004)
7. L. Berge, S. Skupin, F. Lederer, G. Mejean, J. Yu, J. Kasparian, E. Salmon, J.P. Wolf, M. Rodriguez, L. Woste, R. Bourayou, R. Sauerbrey, Phys. Rev. Lett. **92**, 225002 (2004); G. Mejean, J. Kasparian, J. Yu, E. Salmon, S. Frey, J.-P. Wolf, S. Skupin, A. Vinaotte, R. Nuter, S. Champeaux, L. Berge, Phys. Rev. E **72**, 026611 (2005)
8. J. Kasparian, J. Solle, M. Richard, J.P. Wolf, Appl. Phys. B **79**, 947 (2004)
9. P. Sprangle, J.R. Penano, B. Hafizi, Phys. Rev. E **66**, 046418 (2002)
10. S.A. Shlenov, V.Y. Fedorov, V.P. Kandidov, Atmos. Ocean. Opt. **20**, 275 (2007)
11. O.G. Kosareva, V.P. Kandidov, A. Brodeur, C.Y. Chien, S.L. Chin, Opt. Lett. **22**, 1332 (1997); A. Chiron, B. Lamouroux, R. Lange, J.F. Ripoche, M. Franco, B. Prade, G. Bonnaud, G. Riazuelo, A. Mysyrowicz, Eur. Phys. J. D **6**, 383 (1999)
12. S.A. Shlenov, V.P. Kandidov, Atmos. Ocean. Opt. **17**, 565 (2004)
13. E.T.J. Nibbering, G. Grillon, M.A. Franco, B.S. Prade, A. Mysyrowicz, J. Opt. Soc. Am. B **14**, 650 (1997)
14. K.Y. Andrianov, V.P. Kandidov, O.G. Kosareva, S.L. Chin, A. Talebpour, S. Petit, W. Liu, A. Iwasaki, M.-C. Nadeau, Bull. Russ. Acad. Sci. Phys. **66**, 1091 (2002)
15. A.M. Perelomov, V.S. Popov, M.V. Terent'ev, Sov. Phys. JETP **23**, 924 (1966)
16. S.A. Akhmanov, V.A. Vyslouh, A.S. Chirkin, *Optics of Femtosecond Laser Pulses* (American Institute of Physics, New York, 1992)
17. V.P. Kandidov, Uspekhi Fizicheskikh Nauk. **39**, 1243 (1996)